THE ASTRONOMICAL JOURNAL VOLUME 106, NUMBER 4 OCTOBER 1993

STAR FORMATION IN THE DISKS OF H I-RICH S0 GALAXIES[1]

RICHARD W. POGGE
Department of Astronomy, The Ohio State University, Columbus, Ohio 43210
Electronic mail: pogge@payne.mps.ohio-state.edu

PAUL B. ESKRIDGE
Harvard-Smithsonian Center for Astrophysics, Cambridge, Massachusetts 02138
Electronic mail: eskridge@cfa268.harvard.edu

Received 1993 March 12; revised 1993 June 28

ABSTRACT

We present the results of a Hα emission-line imaging survey of a sample of neutral-gas-rich S0 galaxies. We find evidence of disk H II regions in 14 of our sample of 32 galaxies, detect nuclear or faint diffuse circumnuclear Hα+[N II] emission in another 11 galaxies without disk H II regions, and obtain upper limits for 8 galaxies. We find a striking dichotomy between S0's with and without H II regions; either a galaxy has a number of H II regions, most often distributed into distinct rings or ringlike structures, or there are none down to detection limits equivalent to a single unreddened H II region ionized by single O stars. We find that the S0's without disk H II regions have a lower median $M_{\rm H\,I}/L(B)$ than those with disk H II regions, but the distributions have a large range of dispersion. Our data suggest that S0's may lie in a regime where local threshold effects, perhaps primarily kinematic in origin, are more important in determining the star formation in these galaxies than the global stability mechanisms that recent empirical models for large-scale star formation have suggested prevail in later-type spirals.

1. INTRODUCTION

The traditional picture of S0 galaxies as "dead" or "fossil" disk systems with little or no gas, dust, or active star formation has recently been challenged by a variety of observations. Increasing numbers of S0 galaxies have been found to contain significant quantities ($\sim 10^9\,\mathcal{M}_\odot$) of neutral hydrogen (Wardle & Knapp 1986; Chamaraux *et al.* 1986; Eder *et al.* 1991), molecular (CO) gas (Sage & Wrobel 1989; Wiklind & Henkel 1989; Thronson *et al.* 1989; Tacconi *et al.* 1992), and hot ($\sim 10^6$ K) ionized gas (Fabbiano *et al.* 1989, 1992). *IRAS* observations have suggested that a large fraction of S0's have interstellar dust (Jura 1986; Knapp *et al.* 1989). H II regions have been detected in over one-third of the S0 galaxies surveyed using CCD images in the Hα+[N II] emission lines (Pogge & Eskridge 1987; hereafter referred to as PE87). Overall, there is a growing body of evidence to suggest that previous notions about the interstellar medium in these galaxies are in need of revision.

In PE87 we searched for H II regions in 16 S0 and S0/a galaxies. Four of the galaxies had been misclassified as S0 galaxies: two were late-type galaxies with low surface-brightness spiral arms; two were irregular galaxies. The five S0 galaxies with detectable H II regions fell into two groups: three with H II regions organized into ringlike structures, and two with amorphous distributions with no apparent pattern. The integrated Hα luminosities of these galaxies were found to be reduced, but not overwhelmingly so, compared to later-type spiral galaxies (Kennicutt 1983). Because of the small number of galaxies observed, PE87 was more in the character of a discovery paper, establishing that it is reasonable to search for H II regions in systems not previously expected to support ongoing massive-star formation. Our present work includes 24 additional galaxies, bringing us to a sufficient number that we may begin to sensibly address the question of patterns in the distribution and intensity of star formation in S0 galaxies.

This paper is the first in a series exploring the star-formation properties of S0 and S0/a galaxies. In this paper we present the results of our Lick Observatory CCD Hα imaging survey to search for H II regions in 40 S0 and S0/a galaxies with detectable H I 21 cm emission (so-called "gas-rich" S0's). Future papers in this series will discuss the H II region abundances and kinematics, and the results of a Hα imaging survey of H I poor S0's.

Details of our sample selection criteria are given in PE87. Experience with emission-line imaging techniques since PE87 (e.g., Pogge 1989) has lead us to reexamine the results of our earlier work, both in the interpretation and the actual fluxes quoted. In this paper we shall include the revised data from PE87 in the discussion. The basic properties of the combined sample of gas-rich S0 galaxies we shall consider here are listed in Table 1. The primary source of galaxies was the compilation of Wardle & Knapp (1986). The total B magnitude (B_T^0), H I flux (in Jy km s^{-1}), and heliocentric recession velocity (in km s^{-1}) were derived from the Third Reference Catalog of Bright Galaxies (de Vaucouleurs *et al.* 1991; hereafter referred to as RC3). In all cases we consulted the original sources before adopting the RC3 values. The distance listed was derived from the observed heliocentric velocity assuming $H_0 = 75$ km s^{-1} Mpc^{-1} and correcting for Virgocentric infall following the method of Aaronson *et al.* (1982; solution 3.1). Using these distances, we list the total

 0004-6256/93/106(4)/1405/15/$0.90

TABLE 1. H I rich S0 sample.

Galaxy	Type	B_T^0	$V_\odot$[a]	S_{HI}[b]	D_{Mpc}[c]	log $L(B)$[d]	log M_{HI}[e]	Notes
NGC 125	S0$^+$	13.35	5306	0.99	63.9	10.49	8.98	
NGC 160	S0$^+$p	13.06	5255	5.01	70.5	10.69	9.77	
NGC 262	S0/a	14.07	4507	16.2	60.4	10.15	10.1	Tidal Distortion
NGC 473	S0/a	12.50	2129	6.67	28.1	10.11	9.09	PE87
NGC 632	S0?	13.11	3168	4.06	40.6	10.18	9.19	
NGC 670	S0	12.96	3703	4.57	57.5	10.55	9.55	misclassified Sb
NGC 680	S0	12.52	2801	5.25	39.3	10.39	9.28	PE87
NGC 693	S0/a	12.84	1567	11.2	20.2	9.68	9.03	
NGC 694	S0p	13.69	2905	6.17	38.9	9.92	9.34	misclassified Sp (PE87)
NGC 936	SB0$^+$	10.98	1340	6.08	18.0	10.33	8.67	PE87
NGC 984	S0$^+$	14.21	4352	11.5	58.8	10.39	9.97	
NGC 1023	SB0	10.09	637	31.1	11.7	10.31	9.00	PE87
NGC 1167	S0$^-$	12.86	4954	9.20	67.3	10.75	9.99	
NGC 1819	SB0	12.68	4470	3.50	60.0	10.69	9.47	
NGC 2685	S0p	11.86	883	25.4	19.0	10.02	9.33	Polar Ring S0
NGC 2893	SB0	13.76	1699	4.88	32.7	9.74	9.09	
NGC 3413	S0sp	13.07	645	13.8	9.0	8.80	8.33	misclassified Irr
NGC 3593	S0/a	11.50	628	12.3	6.8	9.27	8.13	
NGC 4138	S0$^+$	12.14	923	15.6	23.1	10.08	9.30	PE87, reobserved
NGC 4385	SB0$^+$	12.71	2140	5.01	36.3	10.25	9.19	misclassified SBb (PE87)
NGC 4643	SB0/a	11.59	1399	2.56	27.6	10.56	8.66	
NGC 4670	S0/ap	12.94	1069	1.02	9.6	9.00	7.35	misclassified Irr (PE87)
NGC 4856	SB0/a	11.07	1353	6.55	23.6	10.50	8.93	
NGC 4866	S0$^+$	11.80	1988	16.3	22.2	10.18	9.27	
NGC 5631	S0	12.44	1979	4.37	34.4	10.31	9.09	PE87
NGC 5701	SB0/a	11.69	1506	51.1	28.0	10.43	9.97	
NGC 6501	S0$^+$	12.56	2856	4.29	44.4	10.48	9.30	PE87
NGC 7013	S0/a	10.71	779	21.9	12.9	10.17	8.93	PE87
NGC 7180	S0	13.49	1238	1.24	17.7	9.31	7.96	PE87
NGC 7280	S0$^+$	12.88	1844	1.31	25.5	9.87	8.30	PE87
NGC 7302	S0$^-$	12.91	2586	3.94	32.0	10.18	8.98	
NGC 7679	SB0p	13.01	5138	5.81	60.4	10.56	9.70	
NGC 7742	S0	12.34	1653	10.7	18.9	9.82	8.95	PE87, reobserved
NGC 7743	SB0$^+$	12.18	1662	3.34	21.4	10.00	8.56	PE87
IC 89	S0	13.20	5446	1.08	70.9	10.63	9.11	
UGC 01277	S0/a	13.81	4141	4.02	57.5	10.20	9.50	
UGC 01353	S0$^-$	13.85	5055	6.31	68.4	10.34	9.84	
UGC 12454	S0	14.30	4793	2.19	57.8	10.02	9.24	
UGC 12713	S0/a	14.45	299	9.38	3.3	7.47	8.65	misclassified Irr (PE87)
UGC 12840	S0	13.79	6856	2.47	91.2	10.61	9.68	

Notes to TABLE 1

[a]km s^{-1}, from H I or optical if H I uncertain.

[b]Integrated line flux in Jy km s^{-1} (weighted average following the RC3).

[c]Computed using the Aaronson *et al.* (1982) Virgocentric infall model, sol. 3.1, with $H_0=75$.

[d]$\log L(B)=12.208-0.4B_T^0+\log(1+z)+2\log D_{\rm Mpc}$ in $L(B)_\odot$.

[e]$\log M_{\rm H\,I}=5.372+\log S_{\rm H\,I}+2\log D_{\rm Mpc}$ in $\mathcal{M}_\odot$.

B luminosity and H I mass in solar units. We note in the last column those galaxies that were discussed in PE87, and those galaxies in the combined sample that we judge to have been misclassified as S0's.

In Sec. 2 we describe the new observation and data reduction techniques, and in Sec. 3 we present the results along with a discussion of a few particularly interesting cases. In Sec. 4 we discuss these results, comparing the disk-star-formation properties we observe in the S0 galaxies with those of late-type (Sab to Sc) spiral galaxies, and attempt to understand these galaxies in the context of disk star formation across the Hubble sequence. For simplicity, we shall refer to early type disk galaxies as a group as "S0's," but when referring to individual galaxies, we shall discriminate (as well as possible) between systems classified as S0 or S0/a (and SB0 or SB0/a if barred). By "star formation" we shall mean the formation of massive stars hot enough to provide tracers of their birth in the form of H II regions. Low-mass star formation offers no similarly convenient optical tracer, and only ambiguous tracers at other wavelengths (e.g., *IRAS* colors). Thus, we cannot address the question of the *total* star-formation rate with

these data except via assumptions about an initial mass function—assumptions that may be of questionable validity.

2. OBSERVATIONS AND DATA REDUCTION

2.1 Narrow-band Imaging

All of the new imaging observations were made with the Lick Observatory 1 m Anna Nickel reflector at Mount Hamilton, CA except as noted below. The instrument used was a Cassegrain focal-reducing camera (Stover 1986) with a Texas Instruments 500×500 three-phase CCD detector. This camera/CCD combination uses all-lens optics and provides an unvignetted and undistorted square field of view of about 4.'7×4.'7 with an image scale of ~0.''57/pixel. This TI CCD is a thinned, backside-illuminated device largely free of cosmetic defects. The red narrow-band filter images show no evidence of "fringing" due to internal interference in the CCD.

For each galaxy, a pair of narrow-band images was obtained through 75-Å-wide interference filters isolating the spectral region including the Hα+[N II] $\lambda\lambda$ 6548, 6583 emission lines and a nearby emission-free stellar continuum band. The effective wavelengths of the emission-band filters (6606, 6647, and 6693 Å) were selected to cover the range of redshifts of the sample galaxies. The continuum-band filter has an effective wavelength of 6435 Å and was chosen to be sufficiently near the emission-band filters in wavelength so that spectral color correction terms would be negligible. As a result, the stellar light in the continuum-band images is an excellent representation of the stellar light in the emission-band images. The filters are part of an optically matched (i.e., parfocal) filter set, so there are no changes in effective plate scale between the emission- and continuum-band images. In this instrument the filters were mounted below the focal plane in an $f/17$ beam, so changes in the filter bandpasses due to placement in this slow nonparallel beam are insignificant ($<0.01\%$). Exposure times were 15–30 min in each filter. To provide an absolute flux calibration, white dwarf standard stars from the list of Oke (1971) were observed on each night. Conditions were clear and photometric for the observing runs, with typical seeing between 1'' and 2'' FWHM as measured from field stars on the program images.

2.2 Basic Reduction

Image reduction and analysis was done using the VISTA image processing package (Stover 1988). The image reduction procedures used were effectively the same as those described in PE87, except that we used a faster and more precise technique than cross correlation for registering the on- and off-band images. A marginal sum centroiding technique (Stetson 1979; adapted from Stetson's DAOPHOT package) was used to compare the positions of field stars on the emission- and continuum-band images and thus determine the mean shift between the frames. Using image pairs of galaxies with rich foreground star fields, we verified that there were no relative field rotation or pixel-scale changes between the frames. Image registration is thus accomplished by shifting and rebinning the misaligned image along both axes. A flux-conserving interpolation algorithm was used for the rebinning operation. The typical registration accuracy was ±0.05 pixel, or ±29 mas at our image scale, estimated using the subtraction residuals of field stars. Only the continuum-band images were shifted, and comparison of the pixel statistics in clear-sky regions of the shifted images before and after registration showed little significant smoothing as a result of the rebinning operation.

After registration with respect to the emission-band images, the continuum images were scaled in intensity to create a template for subtracting the starlight component in the emission-band images. The scaling was based on the observations of the standard stars, where the continuum spectrum is known accurately, providing a measurement of the change in instrument efficiency (optics and detector) between the two filter bands. The continuum templates were then subtracted from the emission-band images to produce essentially pure emission-line images of the galaxies. Evaluation of the quality of the subtraction was made based on residuals in the galaxies and the images of field stars on the frames (see Pogge 1992). The set of pure emission-line images produced in this fashion are the basis of the subsequent analysis.

Standard stars were measured by integrating the total signal within synthetic apertures following standard techniques (e.g., DaCosta 1992). Filter transmission curves measured in the laboratory were used to compute the integrated standard-star flux in each filter bandpass, and derive the conversion between instrumental signal in units of DN s^{-1} and total band flux in units of ergs s^{-1} cm^{-2}. Typical fluxes were found to be internally consistent to $\lesssim \pm 5\%$, and the absolute accuracy was $\sim \pm 10\%$ night to night.

Given improvements in our difference imaging techniques as we have gained more experience, we have re-reduced all of the S0 galaxy images described in PE87. This ensures consistency with the present data, and allows us to confidently merge the two datasets. Only minor changes have resulted, although we note that our [N II] correction to the PE87 galaxies has been shown to be consistent with subsequent spectrophotometry and has been revised in this paper. We discovered serious observational errors in the images of two galaxies, NGC 4138 and NGC 7742, during the re-reduction exercise. As a consequence, we recently reobserved these two galaxies with the 1.8 m Perkins Telescope of the Ohio State and Ohio Wesleyan Universities in Flagstaff, AZ using the OSU Imaging Fabry–Perot Spectrograph in direct imaging mode with the etalon removed from the beam (see Pogge *et al.* 1992 for a description of the instrument). These images were obtained as part of a separate study in progress at this writing, but we shall include them here as they will serve to correct two glaring errors in the data presented in PE87.

2.3 Hα Fluxes

Total emission-line counts in units of DN s^{-1} were measured for each of the galaxies from the continuum-

subtracted emission-line images by integrating the emission-line images within minimum flux contours defined to be 3σ above the residual background level. In galaxies where no emission-line regions were detected, upper limits were estimated by computing 3σ detection limits from the residual background statistics within the optical extent of the galaxy (defined by the de Vaucouleurs isophotal radius). We express the upper limit in terms of the Hα emission-line flux of the faintest unresolved H II region we would have detected. A distinction has been drawn between nuclear and disk emission-line regions, as the former may be due to nuclear activity (e.g., Seyfert activity) rather than star formation. Since we are interested in the disk-star-formation properties of these galaxies, we have excluded the nuclear component, if any, from the tabulated Hα emission-line fluxes (see Table 2).

The raw emission-line counts were converted into Hα emission-line fluxes in units of ergs s^{-1} cm^{-2} using a flux scale derived from standard star observations in the emission-line bandpasses. The standard star continuum flux calibration coefficients must be converted into monochromatic calibration coefficients individually for each galaxy to account for both wavelength-dependent filter transmission and for the presence of the [N II] $\lambda\lambda$ 6548, 6583 Å emission lines in the bandpass. The bandpass correction is required as the light from an emission-line region is monochromatic and enters the bandpass at a particular wavelength determined by the galaxy redshift, whereas the light from the standard stars is a continuous spectrum spanning the entire filter bandpass, and so the continuum flux calibration coefficient represents an average over the bandpass. This correction makes use of filter transmission curves measured in the laboratory to provide accurate values of the filter transmission at the emission-line wavelengths of interest.

The [N II] correction was based on independent spectroscopic measurements of the H II regions where available. We shall discuss these spectra in a separate paper. For galaxies without available spectrophotometry, we adopt a value of [N II] λ6583/Hα=0.4, typical of observed disk and nuclear H II regions in our sample (see Table 2). In galaxies where no H II regions have been detected, we compute an upper limit for the detection of a single disk H II region, adopting the 0.4 value appropriate for the disk H II regions that we did detect. Because the [N II] λ6548 and 6583 Å lines have an essentially fixed intensity ratio of $\sim$1:3 (the ratio of the atomic transition probabilities), knowing the [N II] λ6583/Hα ratio and the filter transmission curve is sufficient to estimate the flux of Hα. The derived Hα fluxes (or upper limits) were then corrected for atmospheric extinction using the Hayes (1970) Lick Observatory extinction curve, and for Galactic extinction following Burstein & Heiles (1984), and assuming a Whitford (1958) extinction law as parametrized by Miller & Mathews (1972).

While we correct for Galactic extinction, it is very difficult to apply a correction for extinction intrinsic to H II regions in the individual galaxies. One possible approach would be to apply the "average" intrinsic correction of 1.1 mag (based on radio continuum observations) adopted by Kennicutt (1983). This amount of extinction is consistent with what is derived from the Hα/Hβ Balmer decrements in those of our sample galaxies for which we have spectrophotometry of individual bright H II regions. A comparison of our results for S0's with those of Kennicutt for later-type spirals is at the center of our analysis below, but we note that Kennicutt's Hα fluxes were derived from the observed Hα+[N II] fluxes of Kennicutt & Kent (1983; hereafter referred to as KK83) which themselves were uncorrected for Galactic and intrinsic extinction. Rather than work backwards from Kennicutt's tabulation of the derived Hα fluxes, we started with the observed Hα+[N II] fluxes of KK83 and derived corrected Hα fluxes for 125 spiral galaxies (eliminating irregular and known Seyfert galaxies, and those galaxies which were not detected at Hα). We applied the same Galactic extinction correction as described above for our S0 galaxies, and used the average [N II] correction described by Kennicutt (1983). Since it is the relative comparison that interests us, however, applying Kennicutt's adopted internal extinction value to both samples would only serve to shift the zero point by the same amount, having no effect on the relative fluxes, and so we have not applied this correction. Deriving the Hα luminosities of KK83 spiral galaxies in the same way as we did for our S0's gives us an added measure of consistency, and ensures a fair comparison between the samples.

Intrinsic extinction is the principal source of systematic uncertainty in emission-line imaging studies of H II regions, and in the absence of detailed supplementary data (e.g., thermal radio continuum measurements; Caplan & Deharveng 1986) this is the best we can do for the present. *We reiterate Kennicutt's warning that one should exercise "extreme caution" in considering the Hα fluxes of individual galaxies presented here.* Variations in internal extinction probably imply uncertainties of as much as 50% for individual galaxies. Nonetheless, the statistical properties of the two ensembles should have a smaller uncertainty, and so comparison of the *ensembles* of early and late-type disk galaxies will be the most meaningful.

3. RESULTS

3.1 Disk H II Region Hα Fluxes and Luminosities

For the combined sample of 40 galaxies, 32 galaxies are S0's and 8 have been found to be either irregular, peculiar, or later-type spirals misclassified as S0's. The misclassified galaxies are noted in Table 1, and we describe the reasons for our judgment in Sec. *3.4* below. Of the 32 S0 galaxies, 25 were detected in Hα+[N II] emission. Unambiguous evidence of disk H II regions has been found in 14 of the S0 galaxies. In 11 of the S0 galaxies, 8 have only nuclear emission, and 3 have a combination of nuclear emission and very faint, extended diffuse emission regions of uncertain origin. In these latter three galaxies, the combination of a strong nuclear emission-line source surrounded by a weak, extended diffuse emission component is similar to what is seen in x-ray selected early-type galaxies (e.g.,

TABLE 2. Disk H II region Hα fluxes.

Galaxy	log F(Hα)	log L(Hα)	[N II]/Hα [a]	Emission Region Description
NGC 160	−13.23	40.55	(0.4)	Outer H II Ring
NGC 473	−12.58	40.40	0.47	Inner H II Ring
NGC 632	−12.25	41.04	0.44	Nuclear Starburst
NGC 693	−12.28	40.41	(0.4)	Stubby S-shaped
NGC 1819	−12.14	41.49	0.46	Inner H II Ring
NGC 2893	−13.04	40.07	0.40	Amorphous
NGC 3593	−11.89	39.86	0.36	Inner (nuclear) H II Ring
NGC 4138	−11.87	40.89	0.42	Inner H II Ring
NGC 5701	−12.74	40.23	(0.4)	Outer H II Ring
NGC 7013	−12.84	39.49	0.50	Inner & Outer H II Rings
NGC 7679	−11.87	41.77	0.45	Nuclear Starburst
NGC 7742	−11.98	40.65	0.47	Inner H II Ring
UGC 01277	−13.59	40.01	0.43	Inner H II Ring
UGC 12840	−13.17	40.82	(0.4)	Outer H II Ring
IC 89	< −16.1	<37.7	(0.4)	AGN only (Shuder & Osterbrock 1981)
NGC 125	< −16.1	<37.6	(0.4)	Nuclear emission only
NGC 680	< −15.4	<37.9	(0.4)	
NGC 936	< −15.7	<36.9	(0.4)	
NGC 984	< −16.1	<37.5	(0.4)	Nuclear + faint diffuse emission?
NGC 1023	< −15.1	<37.1	(0.4)	
NGC 1167	< −16.1	<37.6	(0.4)	AGN only (Filippenko & Sargent 1985)
NGC 4643	< −15.7	<37.3	(0.4)	Nuclear emission only
NGC 4856	< −15.9	<36.9	(0.4)	Nuclear emission only
NGC 4866	< −16.0	<36.8	(0.4)	Nuclear + faint diffuse (Shields 1991)
NGC 5631	< −14.9	<38.2	(0.4)	
NGC 6501	< −15.4	<38.0	(0.4)	Faint nuclear emission?
NGC 7180	< −16.2	<36.4	(0.4)	
NGC 7280	< −15.4	<37.5	(0.4)	
NGC 7302	< −15.8	<37.3	(0.4)	Nuclear emission only
NGC 7743	< −15.5	<37.2	(0.4)	LINER (Filippenko & Sargent 1985)
UGC 01353	< −16.1	<37.6	(0.4)	Nuclear emission only
UGC 12454	< −15.9	<37.7	(0.4)	Nuclear emission only

Note to TABLE 2

[a]Values are from unpublished spectrophotometry (Pogge & Eskridge in preparation), and values in parentheses are adopted values when no spectra are available.

Trinchieri & di Serego Alighieri 1991; Shields 1991). For the remaining seven S0 galaxies we have only measured upper limits to Hα+[N II] emission from either the disk or the nucleus.

The integrated Hα fluxes and luminosities of the disk H II regions (or suitable upper limits) for the 32 S0 galaxies are given in Table 2. The first three entries are the logarithms of the derived integrated Hα fluxes (in units of ergs s^{-1} cm^{-2}) and luminosities (in ergs s^{-1}) for the disk, and the observed or adopted [N II]/Hα line ratio. Luminosities were computed using the distances listed in Table 1. If the [N II]/Hα line ratio has been measured spectroscopically, its value is given, otherwise the adopted value is enclosed in parentheses. The upper portion of the table gives the values for the 14 galaxies with detected disk H II regions, and the lower portion gives upper limits for the 18 galaxies with no discernible disk H II regions (estimated as described in Sec. 2.3 above). The last column gives a description of the H II region distribution when H II regions were detected, otherwise a description of what Hα+[N II] emission, if any, was detected is given. For those galaxies with only nuclear emission-line regions, the spectral type of the nucleus (Seyfert, LINER, etc.) is listed if known.

3.2 H II Region Distribution

The distribution of emission-line regions in the galaxies provides us with additional insights into the nature of the star-formation activity in these galaxies. Understanding *where* massive stars form in S0 galaxies will assist us in trying to understand *why* they are forming in the first place. In our sample, the distribution of emission-line regions falls into a few readily discernible patterns.

The most common H II region distribution is apparent H II region rings, seen in 10 of the 14 galaxies with disk H II regions. The properties of these H II region rings are listed in Table 3. For each galaxy with a H II region ring, we list the ring's apparent major axis diameter, D_{ring}, in arcmin, major axis position angle, θ_{ring}, axial ratio (minor/major), Q_{ring}, and the projected radius of the ring, R(kpc). To provide a basis for comparison, we also list the extinction-corrected stellar isophotal major-axis diameter,

TABLE 3. H II region ring properties.

	Galaxy[a]			H II Ring				
Galaxy	$D_0(')$	θ_{25}	Q_{25}	$D_{ring}(')$	θ_{ring}	Q_{ring}	$R(kpc)$[b]	D_{ring}/D_0
NGC 160	2.75	45	0.57	1.43	45	0.48	14.6	0.52
NGC 473	1.74	153	0.63	0.29	145	0.54	1.19	0.17
UGC 01277	1.70	75	0.51	0.49	70	0.17	4.10	0.29
NGC 1819	1.86	120	0.71	0.12	51	0.61	1.05	0.06
NGC 3593	4.90	92	0.37	0.24	90	—	0.24	0.05
NGC 4138	2.40	150	0.66	0.69	146	0.59	2.32	0.29
NGC 5701	4.37	—	0.95	3.65	—	1.00	14.9	0.84
NGC 7013	5.01	157	0.35	1.20	175	0.30	2.25	0.24
				3.84	165	0.33	7.20	0.77
NGC 7742	1.78	—	1.00	0.31	—	1.00	0.85	0.17
UGC 12840	1.26	15	0.89	0.86	—	1.00	11.4	0.68

Notes to TABLE 3

[a]Galaxy data are from the RC3.

[b]Apparent major axis radii were computed using the distances in Table. 1.

D_0, of the $\mu_B=25$ mag arcsec^{-2} isophote in arcmin, the major axis position angle, θ_{25}, and axial ratio of the limiting isophote, Q_{25}, from the RC3. We list the ratio of the ring to galaxy isophotal diameter, D_{ring}/D_0, to give a quantitative idea of the size of the ring with respect to the galaxy. Uncertainties in the diameters are of order $\pm 10\%$, comparable to the tabulated uncertainty of the corrected isophotal diameters given in the RC3. We measured θ_{ring} manually using emission-line image intensity contour maps (the eye does far better than attempting to fit ellipses given the clumpy morphology). The uncertainty in θ_{ring} is typically $\pm 2°$ (estimated by eye), but is probably $\gtrsim \pm 10°$ when the galaxy is nearly round ($Q_{ring} \gtrsim 0.9$).

The ringlike structures we find can be broadly characterized as either "inner" or "outer" rings. Quantitatively, we define inner rings to be those with a ratio of $D_{ring}/D_0 \leqslant 1/3$, and outer rings to be those with $D_{ring}/D_0 > 1/3$. Inner rings occur in 7 of the 10 galaxies with rings, outer rings are seen in 4 of the 10 galaxies, and one galaxy, NGC 7013, has both an inner and an outer ring. In most cases, the inner rings appear near to or within the stellar bulges of the galaxies, whereas the outer rings are clearly associated with the disk of the galaxy. An additional difference is that inner rings tend to be fully filled with H II regions, while outer rings are often more sparsely populated and patchy. Figure 1 shows examples of four inner rings in S0's, and Fig. 2 shows two examples of outer rings.

Irregular H II region distributions are seen in 3 of the 14 galaxies with disk H II regions. There is no discernible pattern to the H II region distributions in these galaxies (excluding galaxies that have turned out to be irregular galaxies misclassified as S0's). A good example of an amorphous distribution in the disk is in NGC 2893 [Fig. 3(a); see also Sec. *3.3*]. The other two galaxies, NGC 7679 and NGC 632, have complex nuclear H II regions dominated by a central brightest H II region and surrounded by a circumnuclear region filled with discrete H II regions [see Figs. 4(a), 4(b)]. Both of these galaxies are UV-excess objects (NGC 632=Mrk 1002, Markarian *et al.* 1977; NGC 7679=Mrk 534, Markarian & Lipovetsky 1973) and have bright semistellar nuclei with H II regionlike spectra that have led to their classification as "nuclear starburst" galaxies (Balzano 1983; Dahari 1985). Because the star formation in these two galaxies appears to be manifestly associated with a nuclear starburst, we shall not include them in our discussion of disk H II region properties below.

Only one galaxy, NGC 693, shows a stubby S-shaped pattern, but that pattern is not very well described as "spiral" in the usual sense one implies when speaking of "spiral arms." The pattern from center to the ends shows only modest twisting ($\Delta\theta = 5°$–$7°$), and does not extend far from the central regions of the galaxy [Fig. 3(b); Sec. *3.3*]. The continuum-band image shows the central regions of this galaxy to be rather dusty, while the outer isophotes have the lenticular appearance characteristic of inclined S0 galaxies [Fig. 3(b)]. Perhaps what we are seeing is an inclined ring or disk broken by dust in the disk.

Finally, we present two examples of S0's in which we do not detect H II regions. The first, UGC 01353, shows a strong nuclear emission-line point source, but pushing the contrast on the continuum-subtracted image [Fig. 5(a)] reveals no discrete H II regions down to the detection limit quoted in Table 2. The second, NGC 984, shows a point-like emission-line nucleus and faint diffuse emission in the inner 15″ [Fig. 5(b)]. The apparent H II regionlike features in the emission-line image are the subtraction residuals of field stars caused by a low-level tracking error occurring during the emission-line image exposure (e.g., the feature about 40″ NW of the nucleus).

3.3 Results for Individual Galaxies

We present below brief descriptions of individual S0 galaxies with disk H II regions. The results for the S0's with H II regions discussed in PE87, except for NGC 4138 and NGC 7742, are not reproduced here. We shall restrict

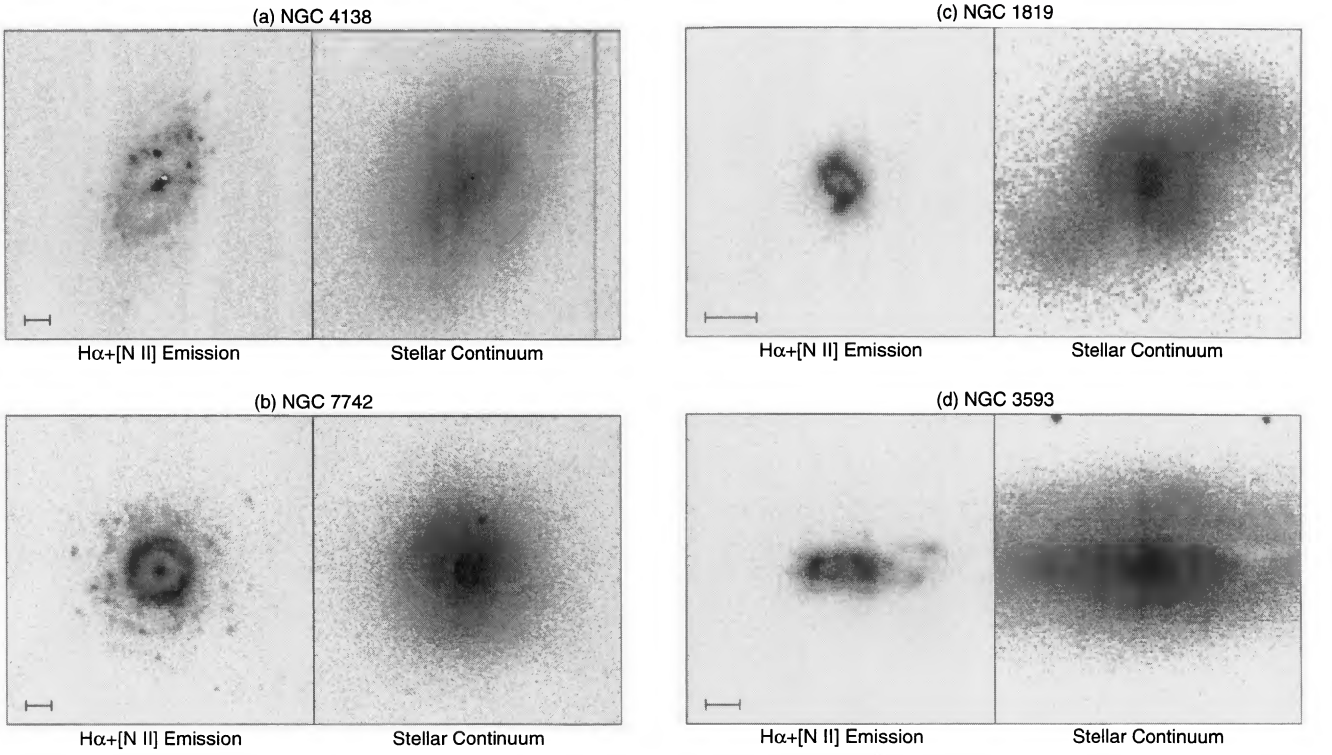

FIG. 1. Examples of four S0 Galaxies with inner H II region rings: (a) NGC 4138 (note the foreground star NW of the nucleus), (b) NGC 7742, (c) NGC 1819, and (d) NGC 3593. In these and subsequent figures, the left panel is the continuum-subtracted Hα+[N II] emission-line image rendered using a linear intensity map, and the right panel is the continuum-band image rendered as a logarithmic intensity mapping (unless otherwise noted). Image orientation is north up, east to the left, and the scale bar indicates 10″ on the sky.

our attention to the true S0 and S0/a galaxies, and will describe the misclassified systems in the following section.

NGC 160. The Hα image [Fig. 2(a)] shows a patchy outer ring of H II regions. The ring region is faintly visible in the continuum band image [Fig. 2(a), right] as a region of slightly higher surface brightness. To emphasize fainter H II regions in the ring, we have increased the contrast in Fig. 2(a), and binned to 1.″2 pixel.

NGC 632. An S0 galaxy with a bright nucleus, the Hα image [Fig. 4(a)] shows a semistellar nucleus surrounded by a complex circumnuclear emission-line region resolved into bright clumps of emission. The circumnuclear H II complex has essentially round outer isophotes, and the 3σ above-background contour has a diameter of 18″; $\sim 0.19\ D_0$ compared to the optical size of the galaxy. The nucleus has a strong H II region spectrum (Balzano 1983), and is an example of a nuclear starburst with considerable circumnuclear star formation.

UGC 1277. A highly inclined S0/a galaxy, it contains an inclined ring of H II regions lying within the inner third of the galaxy. The inclination is not so large as to obscure the H II regions behind the dust lane, though the total Hα luminosity may be underestimated due to extinction in the dusty regions.

NGC 693. The Hα image of this S0's galaxy [Fig. 3(b)] shows a bright nucleus and an S-shaped distribution of H II regions. This complex extends no further than 23″ from the center along the major axis, still falling well within the inner confines of the galaxy ($D/D_0 = 0.36$). The major axis

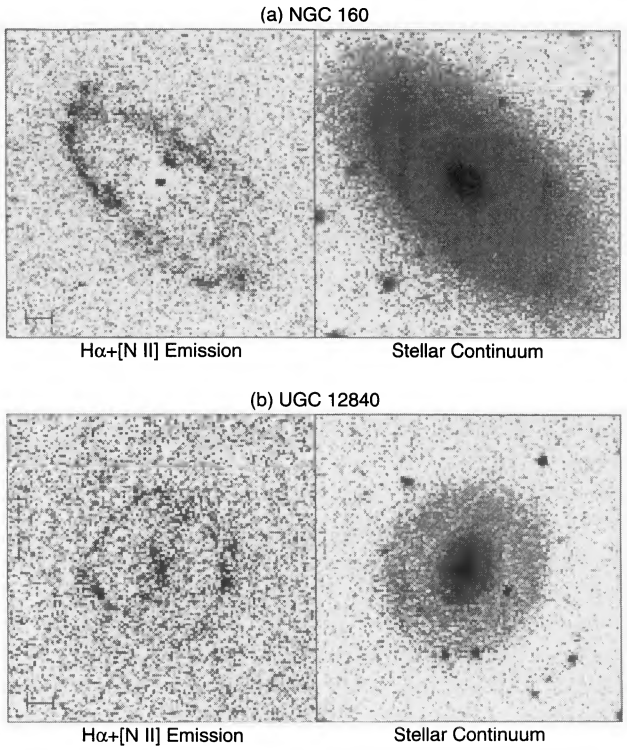

FIG. 2. Examples of two S0 Galaxies with outer H II region rings: (a) NGC 160, and (b) UGC 12840. The higher noise in the Hα image of UGC 12840 is due to an electronics problem during the emission-band image readout. Orientation and scale are as in Fig. 1.

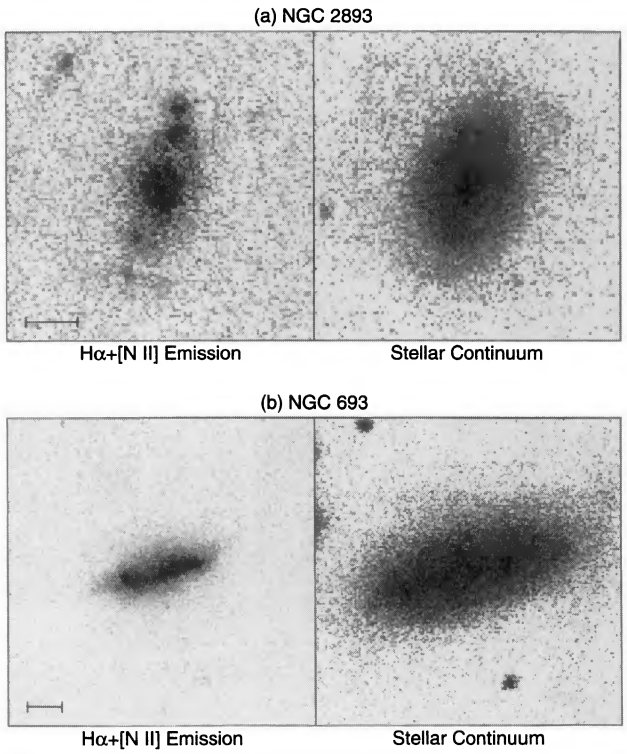

FIG. 3. Examples of two S0 Galaxies with irregular H II region distributions: (a) NGC 2893 (note the bright nucleus), and (b) NGC 693 (note the dustiness of the inner regions on the continuum image). Orientation and scale are as in Fig. 1.

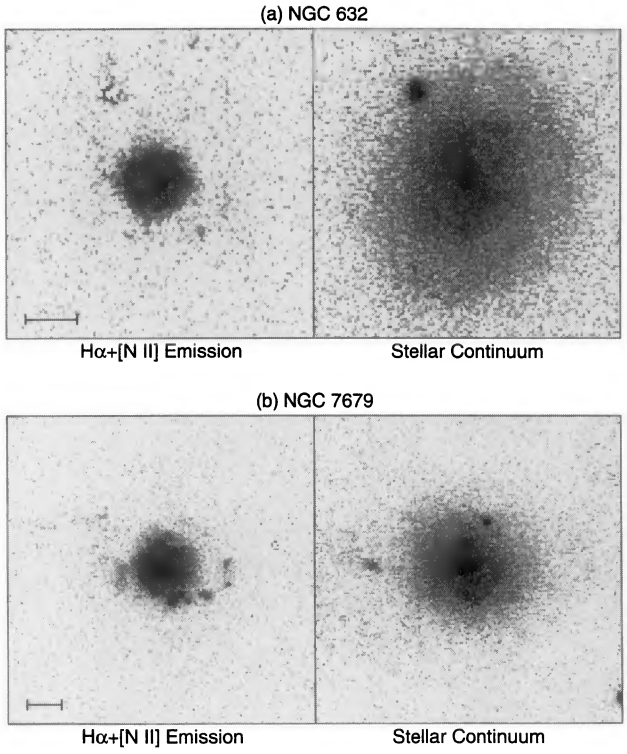

FIG. 4. Two S0 Galaxies with nuclear starbursts: (a) NGC 632 (Mrk 1002) and (b) NGC 7679 (Mrk 534). Orientation and scale are as in Fig. 1. Because of the broad range of emission-line intensities, a logarithmic stretch has been used for the Hα+[N II] emission-line images.

of the pattern lies along position angle 106°, the same as the major axis of the $B=25$ mag arcsec^{-2} isophote. Unlike the apparently misclassified spirals in the sample, there is no suggestion of the spiral pattern in the continuum image of the galaxy.

NGC 1819. A SB0 galaxy, the Hα image [Fig. 1(c)] reveals a small ring of very bright H II regions in the inner regions, well within the stellar bar. The ring of H II regions is dominated by two bright complexes roughly opposite each other across the ring, and the rest of the ring is filled in by fainter regions. The two bright complexes are sufficiently luminous for this galaxy to be identified as a UV-excess source (Mrk 1194; Markarian *et al.* 1979). There is no suggestion of any nuclear emission source, nor are any H II regions detected further out in the disk. The bright inner ring resembles what is seen in the anemic SBa galaxy NGC 4314 (Benedict 1980), but NGC 1819 is of an earlier Hubble type and considerably more luminous ($M_B^0=-22.1$ compared to -18.7 for NGC 4314).

NGC 2893. This galaxy has a bright semistellar nuclear emission-line source with an H II regionlike spectrum, and has been identified as a UV-excess source by Markarian & Lipovetsky (1971; Mrk 401). Most of the Hα emission is concentrated into the inner 28″ of the galaxy ($D/D_0=0.42$), and dominated by the nuclear emission, though discrete bright H II regions can be seen along the major axis of the inner stellar isophotes [Fig. 3(a)].

NGC 3593. A nearby, nearly edge-on S0/a galaxy, the H II regions in the inner parts of this galaxy were previously studied by Hunter *et al.* (1989). They have characterized NGC 3593 as "peculiar," although we find nothing unusual about this galaxy. Our Hα image [Fig. 1(d)] shows the emission to be concentrated into two very bright H II complexes along the major axis, and with numerous minor complexes filling in what appears to be a rather inclined H II region ring. The inclination is apparently not so large as to cause the central H II ring to be obscured by the dust lane that gives this galaxy its S0/a classification.

NGC 4138. This galaxy was originally described by PE87, but the data were of poor quality. During our reanalysis of the PE87 images for this paper, we found that the nucleus was strongly distorted by the presence of a foreground star that was slightly brighter than the nucleus and separated by only ~4″. The combination of poor seeing (2.″7) and the finer sampling (0.″26/pixel) of the GEC CCD used for these images caused a great deal of trouble. Thus, we reobserved this galaxy with the OSU IFPS, and present the new images in Fig. 1(a). The problem was primarily in the nuclear regions, and with better seeing we confirm the ring of the bright H II regions in the disk reported in PE87, resolving many blobs into discrete regions, and detecting many fainter regions. The integrated Hα flux reported in PE87, however, is in error by a factor of ~3, and we give the revised value in Table 2.

NGC 5701. This galaxy is a nearly face-on SB0/a galaxy with a faint nuclear source and a large, sparse ring of H II regions in the outer disk of the galaxy, well beyond the bar

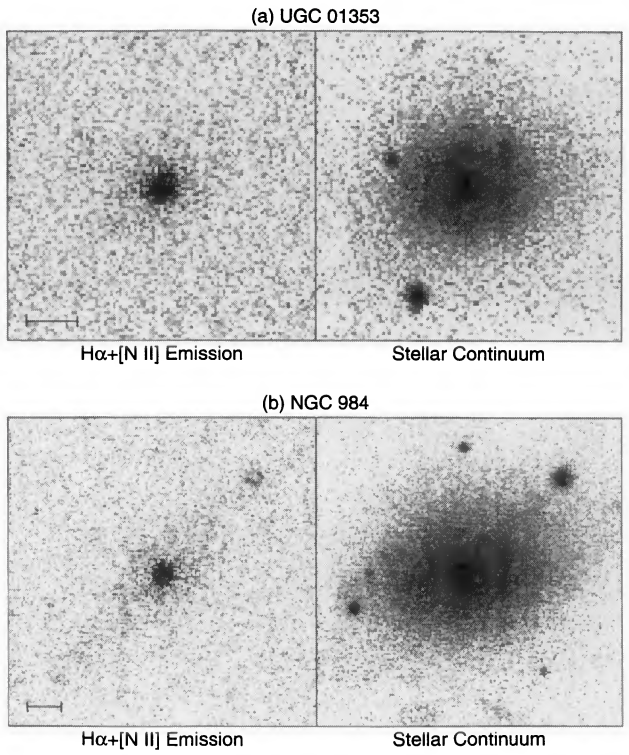

FIG. 5. Examples of two S0 Galaxies with no disk H II regions detected: (a) UGC 01353, showing only a stellar emission-line nucleus; (b) NGC 984, showing a stellar nucleus and a slight hint of extended diffuse emission. Orientation and scale are as in Fig. 1.

($D_{\rm ring}=0.84\ D_0$). Like NGC 160, the outer ring region is also faintly visible in the continuum image, and on the POSS plates.

NGC 7679. A peculiar SB0 galaxy showing tidal distortion because of interaction with a faint companion about 1′ east, our Hα image [Fig. 4(b)] reveals a luminous nuclear star-formation complex resolved into bright clumps of emission with an apparent spiral-like spur running off toward the southwest to west. The brightest circumnuclear H II complex has essentially round outer isophotes with a 3σ above-background isophote diameter of 18″ ($\sim 0.22\ D_0$). The nucleus has a strong H II regionlike spectrum (Dahari 1985), and like NGC 632 is an example of a nuclear starburst with considerable circumnuclear star formation.

NGC 7742. In PE87 we reported that NGC 7742 had a faint, amorphous emission-line distribution, but upon reexamination of those data we found that we were seriously in error: NGC 7742 has a small, bright inner H II region ring. We were fooled because the [N II] λ6548 emission line contaminated our off-band filter image, strong [N II] λ6583 emission dominated the emission-line flux in the on-band filter image, and Hα fell onto the blue wing of the on-band filter. The combination of these unfortunate circumstances resulted in our subtracting away most of the emission-line flux in the on-band image with the scaled "off-band" image. To correct this, we reobserved NGC 7742 using the OSU IFPS, and present the new images in Fig. 1(b). The bandpass was chosen to eliminate the contamination problem, and the new images show clearly a bright ring of H II regions and many fainter disk H II regions beyond the radius of the ring. A revised Hα flux measured from this image is given in Table 2.

UGC 12840. A distant ($\sim$91 Mpc) and luminous ($M^0_B=-21.7$) face-on SB0 galaxy, it appears to be a distant analog of NGC 5701 described above. It shows an outer ring of H II regions lying at $D_{\rm ring}=0.68\ D_0$, well outside the inner stellar bar [Fig. 2(b)]. The galaxy also has a bright nuclear emission-line source of unknown spectral type. Like NGC 160 and NGC 5701, the outer H II ring region is marginally discernible in the continuum image [Fig. 2(b), right], but this requires deeper broadband images to confirm. The greater noise in Fig. 2(b) is a result of an electronics problem that increased the effective readout noise of the emission-band image. The images were binned to 1.″2 pixel to mitigate the problem.

3.4 Misclassified or Anomalous Galaxies

One of the difficulties of studying the properties of S0 galaxies is the problem of morphological classification of the galaxies. Despite serious efforts to weed out misclassified systems from large samples (e.g., Wardle & Knapp 1986), later-type spirals and irregular galaxies turn up in detailed studies of S0's. In our sample of 40 S0 galaxies, six galaxies are clearly misclassified and two are very peculiar. We describe them briefly here with our reasons for either reclassifying them or rejecting them from further discussion on the grounds of anomalous morphology. The first four below we revisit from PE87, while the last four are new to this study.

NGC 694 (Mrk 363). In PE87, we argued that this galaxy is a S0, but subsequent better quality imaging suggest to us that this galaxy is truly anomalous and is more properly classified as a peculiar late-type starburst galaxy. We base our change in classification primarily on the deep *I*-band image of this galaxy of Smith (1988) that shows faint spiral arms extending quite far from the inner region we discussed.

NGC 4385 (Mrk 52). This galaxy studied in PE87 is manifestly a later-type spiral, probably SBb or SBbc, but with much weaker arms than is typical of these classes. While included in the discussion of PE87, we will discuss it no further here.

NGC 4670. This galaxy was classified as an Irregular galaxy by Sakka *et al.* (1973), and while included in PE87, we will not include it here.

UGC 12713. In PE87, we reclassified this galaxy as Irregular on the basis of its optical morphology. Subsequent H I mapping by van Driel & van Woerden (1991) shows a compact, ragged neutral gas distribution with a "small" velocity range [Fisher & Tully (1981) report a velocity width of 115 km s^{-1}, consistent with the isovelocity contours shown by van Driel & van Woerden]. While they have classified it conservatively as S0?, we maintain our Irr classification, especially given the very low intrinsic luminosity ($M^0_B=-13.1$, the same as the Leo A dwarf irregu-

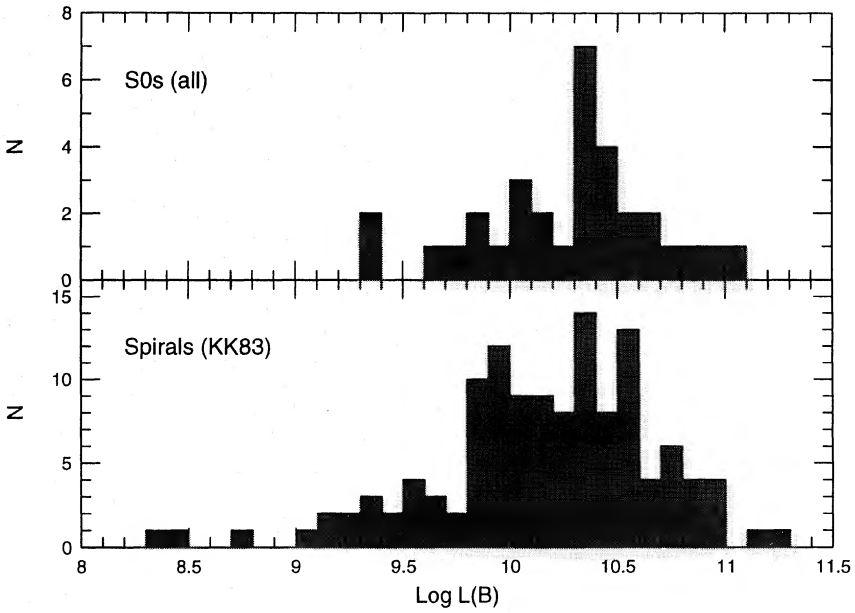

FIG. 6. Distribution of log $L(B)$ (corrected for extinction and color effects) for the gas-rich S0 sample (top) and for 125 spiral galaxies observed by Kennicutt & Kent (1983) (bottom).

lar, Krann-Korteweg & Tammann 1979), and low H I velocity width.

NGC 262 (Mrk 348). This is a tidally distorted galaxy (Simkin *et al.* 1987) with a strong Seyfert 2 nucleus (e.g., Koski 1978). Our images of this interacting galaxy show long, faint spiral arms that appear to be tidally stretched toward its east companion. This galaxy may once have been S0, but its tidal peculiarity lead us to eject it from the sample on the grounds of highly anomalous morphology.

NGC 670. Our Hα+[N II] images show copious H II regions across the disk, and we note that the Revised Shapley Ames catalogue (Sandage & Tammann 1987) classifies it as Sb(s)I, in contrast to the S0 classification given in the RC3. We support the RSA classification of Sb, primarily on the basis of the rather flocculent appearance of the spiral structure outlined by the H II regions.

NGC 2685. This galaxy is a member of the rare class of Polar Ring Galaxies (Whitmore *et al.* 1990), and while there is little doubt that the main galaxy is a S0, its overall morphology is manifestly due to an unusual tidal interaction, and sufficiently anomalous for us to reject it from further consideration in this paper.

NGC 3413. While it looks like a spindle-type lenticular (e.g., the classification in the RC3), it is better classified as amorphous irregular (Hunter 1992), especially given its low intrinsic luminosity ($M^0_B = -16.7$) which is comparable to that of the SMC ($M^0_B = -17$; Krann-Korteweg & Tammann 1979).

4. DISCUSSION

4.1 Comparison with Spiral Galaxies

The KK83 sample of spiral galaxies is well suited for comparison with our S0 galaxy sample as both samples turn out to have similar distributions of integrated B luminosity (corrected for inclination effects following the RC3). This is of concern as a common problem encountered when comparing the properties of two samples of galaxies is the "richness" bias due to the fact that intrinsically larger galaxies tend to have more of all galaxian components (stars and ISM). The distributions of $L(B)$ for our S0 sample and for the KK83 spirals sample are shown in Fig. 6. The median $L(B)$ of the S0 sample is about 24% brighter than the median $L(B)$ for the KK83 sample [2.14×10^{10} $L(B)_\odot$ for the S0's compared to 1.74×10^{10} $L(B)_\odot$ for the spirals], but a Mann–Whitney (hereafter referred to as MW) U test (Siegel 1956) only accepts the hypothesis that these two samples have significantly different medians at the 66% confidence level, and a Kolmogorov–Smirnov (hereafter referred to as KS) test allows us to reject the hypothesis that the two samples have the same $L(B)$ distributions at only the 56% confidence level. This allows us to establish with confidence that any subsequent differences in secondary integrated absolute properties [e.g., $L(\mathrm{H}\alpha)$ or $M_{\mathrm{H\,I}}$] found between these two samples are likely to be measuring real differences, and not subject to a richness bias because one or the other sample has been drawn from an intrinsically more or less luminous parent population.

Figure 7 shows the distribution of the integrated disk Hα luminosities (or upper limits) for the S0 galaxies (top panel) and the KK83 spirals (bottom panel). The two nuclear starburst galaxies (NGC 632 and NGC 7679) are included in the top panel for completeness, but will be omitted from the subsequent discussion. The median $L(\mathrm{H}\alpha)$ for the S0 galaxies with H II regions is 2.51×10^{40} ergs s^{-1} compared to 7.41×10^{40} ergs s^{-1} for the KK83 sample. A MW U test shows that the factor of $\sim$3 lower

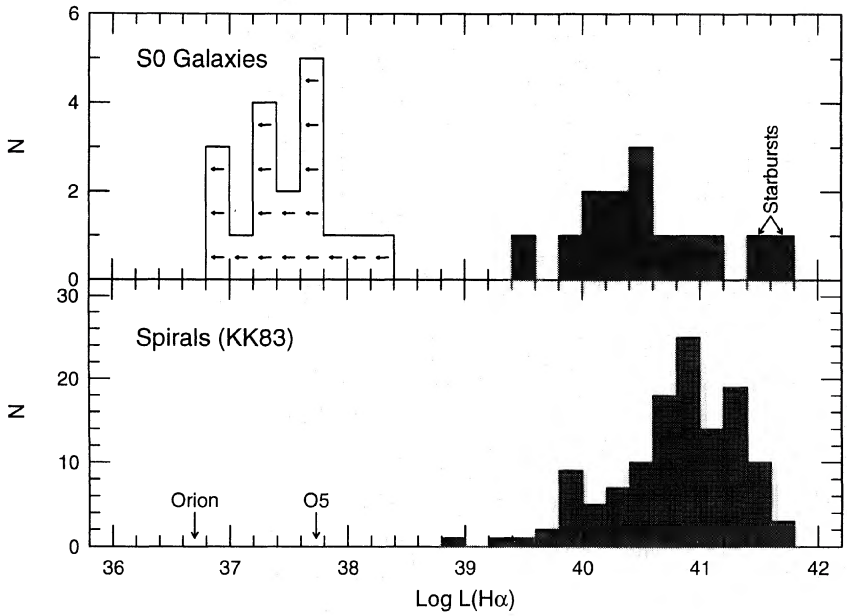

FIG. 7. Distribution of log $L(\mathrm{H}\alpha)$ for the gas-rich S0 sample (top) and the KK83 spirals (bottom). The two starburst galaxies (NGC 632 and NGC 7679) are labeled at the extreme left of the top panel. Upper limits are shown for the S0 galaxies with no disk H II regions. The predicted luminosity of an ideal H II region ionized by a single O5 V star and the observed luminosity of the Orion Nebula are indicated with arrows in the lower panel.

median $L(\mathrm{H}\alpha)$ of the S0 sample is statistically significant at the $>99\%$ confidence level. To provide some physical intuition to aid in the interpretation of the lower limits listed in Table 2 and shown in Fig. 7, we have indicated the predicted $L(\mathrm{H}\alpha)$ for an ideal ionization-bounded H II region excited by a single O5 star, and the observed $L(\mathrm{H}\alpha)$ for the inner core of the Orion Nebula (Pogge *et al.* 1992) with the arrows in the bottom panel. The predicted luminosity of a H II region ionized by a single O5 star is $\sim 6.7\times 10^{37}$ ergs s^{-1}, assuming case B recombination (e.g., Osterbrock 1989) for typical nebular parameters and adopting the number of Lyman continuum photons expected from a O5 ZAMS star given by Panagia (1973). The excitation of the visible portion of the Orion Nebula is dominated by a single star, θ^1C Orionis, that has been classified as O7 V by Conti (1973). The unreddened $L(\mathrm{H}\alpha)=5.4\times 10^{36}$ ergs s^{-1} of Orion is consistent with what would be predicted using Panagia's tabulated Lyman continuum photon flux for a O7 V star.

The most striking feature of the distribution of $L(\mathrm{H}\alpha)$ in the gas-rich S0 galaxy sample (Fig. 7) is the wide gap between the S0's with H II regions and the S0's with only upper limits. This illustrates graphically the effect noted earlier: either we observe a number of H II regions in S0's (most often organized into ring or ringlike structures with a restricted range of galactocentric radii), or we observe none at all. The typical Hα upper limits measured from the emission-line images of the S0 galaxies without disk H II regions (Table 2) are comparable to failure to detect a *single* unreddened H II region excited by one or a few O7 to O5 stars.

4.2 Comparison with H I Properties

The comparison of the relative amounts of H I gas in the KK83 spirals and the S0's with and without H II regions is quite revealing. In Fig. 8 we show the distribution of $M_{\mathrm{H\,I}}/L(B)$ for these three groups of galaxies, marking the medians with arrows. The neutral gas content relative to total starlight decreases from a global median of 0.20 for the spirals to 0.13 for the S0's with H II regions. A MW U test indicates that this difference is significant at the $>96\%$ confidence level. A substantially greater difference, however, is apparent when we compare the KK83 spirals with the S0 galaxies without detected disk H II regions, where the median $M_{\mathrm{H\,I}}/L(B)$ drops to 0.05, or a factor of ~ 4 reduction in the global H I gas content relative to stellar content compared to the KK83 spiral sample. A MW U test here shows that the lower median for the S0's without disk H II regions is significant at the $>99.9\%$ confidence level. Further, differences between the median $M_{\mathrm{H\,I}}/L(B)$ between the S0's with and without H II regions is significant at the $>98\%$ confidence level. A comparable battery of KS tests shows similarly that the apparent differences between the three samples are significant at the $>99\%$ level, except for the KK83 spirals against the S0's with disk H II regions, where the null hypothesis is rejected at a marginal 93% confidence level. While the median $M_{\mathrm{H\,I}}/L(B)$ is significantly lower in the S0's without H II regions compared to those with H II regions, there is considerable overlap between the two distributions. An unfor-

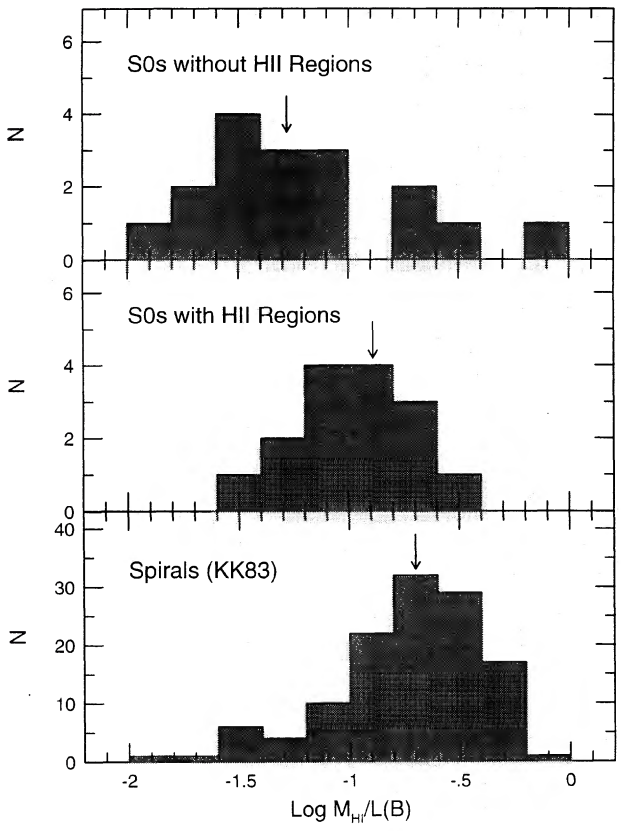

FIG. 8. Distribution of $\log M_{\rm H\,I}/L(B)$ for (top) gas-rich S0 galaxies without disk H II regions, (middle) gas-rich S0's with disk H II regions, and (bottom) the KK83 spiral galaxies. The median $M_{\rm H\,I}/L(B)$ for each sample is marked with an arrow.

tunate choice of galaxies in a similar imaging study of only a few galaxies could have potentially yielded the opposite result.

Often the H I data are used with the Hα luminosities to estimate a gas depletion time from a Hα-derived estimate of the instantaneous star formation rate (cf. Kennicutt 1983; PE87). Unlike Sc's or Irr's, where the star-formation regions cover much of the galaxies, the H II regions in the S0 galaxies studied here are strongly localized radially, making it very difficult to interpret a gas depletion timescale derived in the usual way. Most of the H I gas in the S0's could easily lie well away from the star-forming regions. Further, the most relevant ISM phase for star formation is probably H_2, not H I, and we know even less about the distribution of molecular gas in S0's than we do about the H I gas. Only a few S0's have been studied in sufficient detail to even detect them in CO emission, much less to map them. Of the true 32 S0 galaxies in our sample, only five have been detected in CO $J=1\rightarrow0$ emission, and none have been mapped. Of the five, two are nuclear starburst galaxies with significant but unconfirmed detections (NGC 1819; Thronson *et al.* 1989, and NGC 7679; Wiklind & Henkel 1989), one is an unconfirmed marginal 3σ detection (NGC 4138; Thronson *et al.* 1989), and the final two were detected by both Thronson *et al.* (1989) and Wiklind & Henkel (1989), but NGC 7013 is a factor of 10 discrepant marginal 2σ detection, and NGC 3593 is a factor of 4 discrepant 5σ detection. It is still too early to say much about the molecular content of S0 galaxies. Until the nature of the spatial correlation (if any) of the atomic, molecular, and ionized gas is clarified by high-resolution H I and CO mapping of these galaxies, we cannot sensibly address the possible history of the ongoing star formation in these S0's relative to gas content using depletion timescale arguments.

4.3 Comparison With Far-IR Properties

IRAS far-IR fluxes are available from the literature for 118 of the KK83 spiral galaxies and 29 of the S0 galaxies in our sample (Rice *et al.* 1988; Knapp *et al.* 1989; Fullmer & Lonsdale 1989; RC3). Of the S0 galaxies, 23 were detected in both the 60 and 100 μm bands, while only upper limits to the flux in one or both bands were measured for the remaining six. Because of the small number of S0 galaxies and the large fraction ($\sim$20%) of upper limits, we compared these samples by computing their Kaplan–Meier (hereafter referred to as KM) distribution functions, a technique that treats the upper-limit values explicitly (Feigelson & Nelson 1985). The KM distributions of $\log L_{\rm FIR}/L_B$ for the S0 galaxies with H II regions (13 galaxies including 2 upper limits) and the KK83 spiral galaxies are indistinguishable, having KM distribution means of $\overline{\log L_{\rm FIR}/L_B}=0.271\pm0.163$ and 0.272 ± 0.026, respectively. By contrast, the corresponding KM distribution function for the S0's without disk H II regions (16 galaxies including 4 upper limits) is shifted to significantly lower values ($\overline{\log L_{\rm FIR}/L_B} = -0.792 \pm 0.171$).

If we adopt the hypothesis that the majority of the far-IR radiation from star-forming galaxies is thermal emission from dust grains heated by hot stars, then the lower mean $L_{\rm FIR}/L_B$ for the S0's without H II regions is consistent with our Hα imaging results. Because the *IRAS* data are spatially unresolved, however, there is no clear way to disentangle the far-IR emission due to star formation from that expected from possible active nuclei or grains heated by the interstellar radiation field in those galaxies. Since we have only a small number of S0 galaxies, with several far-IR flux upper limits, we conclude that while the *IRAS* results are reassuring, they tell us nothing further about the star-formation properties of these galaxies. Given the highly localized nature of star formation in these galaxies, an adequate understanding of the relationship between their star-formation activity and the far-IR emission will require far-IR imaging at resolutions comparable to those of our Hα images.

4.4 Massive Star Formation in S0's

The prevalence of H II region rings in our sample is an important morphological clue to the reasons why stars are forming in these galaxies. We would not expect such a high degree of spatial organization if star formation was purely stochastic in these galaxies. Looked at carefully, what appears to be a ring is probably better prescribed as tightly

wound spiral arms, similar to the structures seen in the inner regions of later-type spirals (Buta 1986; Pogge 1989). While we currently lack the necessary data to confirm that these rings represent kinematically distinctive regions as in later-type spirals, we shall adopt it as a reasonable working hypothesis. Under this assumption, the rings in the star-forming S0's play the same role as spiral arms in later-type galaxies; they serve as agents for the aggregation of sufficient gas to lead to star formation (e.g., Larson 1988), even if they may not be the actual "triggers" of such activity through spiral density wave shocking of the gas. Since S0's have very little gas to start with, some kinematical assistance seems to be required to gather enough material together to form stars. What role does an aggregation mechanism play in determining the star-formation properties of these gas-rich S0's?

Following a suggestion by Quirk (1972), Kennicutt (1989) demonstrated a remarkable correlation between the radii in a galaxy at which H II regions are found (in an azimuthally average sense) and the radii at which the local gas surface density in above a critical "threshold" surface density at which a thin, self-gravitating gas disk becomes unstable (e.g., Toomre 1964). In regions where the gas surface density is well above the critical density, the SFR–density relation is nearly linear and star formation is probably self-regulating and largely stochastic. Near the threshold density, the SFR–density relation becomes strongly nonlinear and star formation is probably locally induced, primarily by compression (e.g., induced in spiral arms by either spatial density-wave shocking or aggregation of clouds), while below the threshold density, global star formation is suppressed entirely. Traditional Schmidt-Law SFR–density relations (Schmidt 1959) are pure power laws in which star formation tends to fade away rather than cutoff abruptly unless an ad hoc threshold density is introduced to create such a cutoff. In the disk stability picture, the threshold density is a natural consequence of the model, but not a universal constant; it depends on the overall kinematic properties of each galaxy, giving it a strong radial dependence through the radial dependence of the epicyclic frequency and rotation speed. This picture provides a natural explanation for the apparent suppression of global star formation in gas-rich S0 galaxies: for five S0 galaxies mapped by van Driel (1987), Kennicutt showed that the azimuthally averaged H I surface density falls well below the critical density threshold (see Fig. 17 of Kennicutt 1989).

While a subthreshold gas disk would be stable and act to suppress *global* star formation in this picture, this does necessarily not rule out the possibility of *local* star formation. If the rings of H II regions we see are associated with the Lindblad resonances in the galaxies, then the aggregation of gas by the action of these rings could boost the local gas density into the nonlinear response regime of the SFR–density law. Further, because S0's are rather rapidly rotating, the critical density is higher and so the jump in SFR near the threshold will be expected to be much larger, making the contrast between galaxy disks with and without star formation very strong. Thus, Kennicutt's disk instability picture can perhaps explain the two principal features we see in our sample of S0 galaxies: the strong radial dependence on star formation manifest as prominent rings of H II regions, and the striking dichotomy in star formation activity between S0's with and without H II regions.

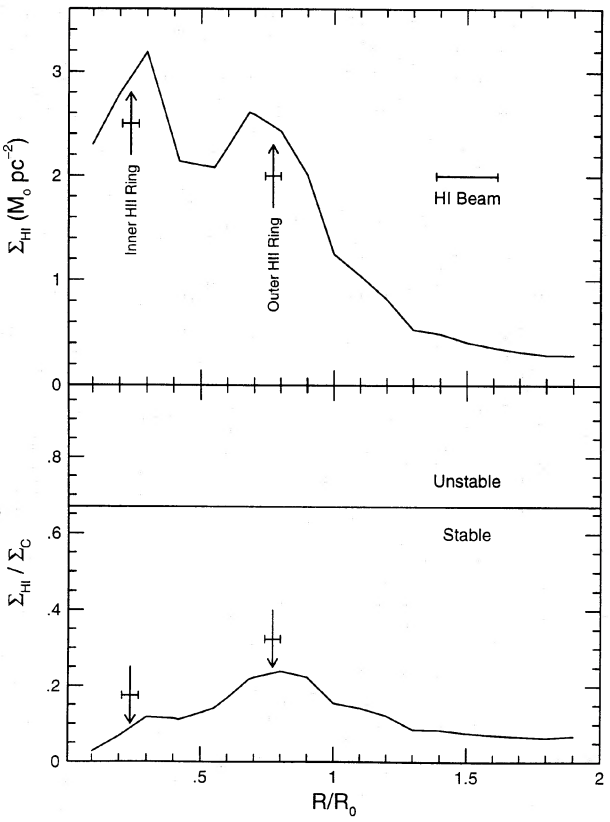

FIG. 9. Azimuthally averaged H I surface density profiles as a function of isophotal radius, R_{25}, for NGC 7013 from the data of van Driel & van Woerden (1991). The top panel plots the H I surface density in units of $\mathcal{M}_\odot$ pc^{-2}, and the bottom panel shows the ratio of the H I surface density to the critical density for gas disk stability, Σ_C, computed using the observed rotation curve following Kennicutt (1989). The radii and extents of the H II region rings reported by PE87 and the half-power beam width of the H I observations are indicated in both panels. The horizontal line in the lower panel is the empirical stability threshold found by Kennicutt for late-type spirals.

In our sample of S0 galaxies with disk H II regions only one, NGC 7013, has a sufficiently detailed H I map (van Driel & van Woerden 1991) to allow us to carry out a stability analysis following Kennicutt (1989). This galaxy has two H II region rings: a complete inner ring and a sparse outer ring. In Fig. 9 we plot the radial dependence of the azimuthally averaged H I surface density [Fig. 9(a)], and the ratio of the gas density with respect to the critical density for stability, Σ_C [Fig. 9(b)] for NGC 7013. At all radii, the gas surface density lies below Σ_C, and the disk is thus globally stable by Kennicutt's criterion. At the radii of the two H II region rings, however, there are distinct peaks in the gas surface density. It may be that the gas surface density at these locations is strongly peaked and closer to Σ_C, but it is being smoothed by the large beam of the H I

map. Ideally, we would want a H I map with spatial resolution comparable to the scale of the inner and outer H II regions rings, combined with a similar CO map to provide an estimate total atomic and molecular gas surface density is in this galaxy. At present, however, there are only two marginal (2σ) and highly discrepant large-beam detections of the CO $J=1\rightarrow0$ emission line from NGC 7013 (Thronson *et al.* 1989; Wiklind & Henkel 1989), so we can say very little about its molecular content. While inconclusive, the available data do seem to lend at least partial credence to our suggestion that the star formation in these regions is being regulated by local effects rather than global instability.

In dwarf irregular galaxies the ratio of rotational to random velocities is much lower than in spirals or S0's, and Skillman *et al.* (1987) have found that a threshold surface density of $\Sigma_{\rm H\,I}\sim10^{21}$ cm^{-2} (averaged over $\sim$500 pc) is required to trigger star formation. Such a *local* triggering threshold is perhaps more relevant to S0 galaxies than the global threshold discussed above, although the actual threshold will likely be complicated in S0's by rotational shear in the gas disks, especially near the Lindblad resonances that we suggest are responsible for the H II region rings we observe. Measuring $\Sigma_{\rm H\,I}$ in our sample of S0 galaxies at the same spatial resolution as Skillman *et al.* requires H I maps with angular resolutions ranging from 15″ for NGC 3593 to $\sim$1.″1 for UGC 12840. Thus, at least for the most nearby S0 galaxies in our sample, we can obtain the necessary resolution with existing facilities.

5. CONCLUSIONS AND FUTURE WORK

A final conclusion we draw from this study is that what all of the available data are telling us is that the star formation in these gas-rich S0's is *normal*, and follows the general trend of decreasing star-formation activity observed along the Hubble sequence (Kennicutt *et al.* 1989). While one does not expect that such a complex phenomenon is a simple one-parameter family, it is possible that there is an important guiding parameter, namely the relative importance of global vs local instabilities in the gas disks in regulating the degree of star formation in a given Hubble type. Sc and later-type galaxies are globally unstable over most of their extent, reflected in the broad radial distribution of H II regions. As we proceed towards the earlier-type disk galaxies, the gas disks become increasingly more stable, and the star formation comes to rely increasingly on local effects (e.g., spiral arms or resonances) to occur. When we reach the earliest disk galaxies, we are in the regime where the gas density is mostly subthreshold except for local regions where one is in the strongly nonlinear near-threshold regime. Here we see the striking dichotomy between gas-rich S0's with and without disk H II regions. In this regime, one expects a substantially greater sensitivity to the overall gas distribution within the galaxy. As the regions where stars can form become more highly localized in radius, the amount of gas available and where it is located in the galaxy becomes even more critical. This may be why we see S0's devoid of H II regions that are more gas rich than galaxies that have H II region rings (Fig. 8). The nonlinearity of the star-formation mechanism at the local scale in near-threshold gas is manifest in this dichotomy: we do not see the star-formation activity simply fading away, leaving behind one or two lone H II regions before fading out altogether.

Much work remains to be done to clarify the vague outlines we are beginning to discern of the nature of star formation in S0's, and its relation to star formation along the Hubble sequence. One key question that our morphological and flux data cannot address is the origin of the gas that is forming stars. It may be that S0's may only form stars if there is a boost to the gas content during the tidal capture of a dwarf galaxy, as suggested by some of the H I morphology studies (e.g., van Driel & van Woerden 1991). Since we see H II regions, the next step is to investigate their nebular abundances via optical spectrophotometry: if the gas originated from a dwarf galaxy we should see the imprint of this origin in reduced O/H abundances. This is the subject of the next paper in this series.

While the apparent correlation between low $M_{\rm H\,I}/L(B)$ and absence of disk H II regions is interesting, it is also difficult to interpret. Again, the reason is that the star formation is highly localized, but the H I measurements are global, and in many cases much of the H I gas is in the outer regions of the galaxies (van Driel & van Woerden 1991). Further, it is well known that molecular gas may play a more intimate role in massive-star formation (and indeed in star formation in general) than neutral hydrogen, and so by assaying only the H I gas content we are ignoring a potentially more relevant ISM constituent. At present, we cannot address the relation between the presence or absence of disk H II regions in S0's vis-a-vis their molecular (or, ideally, total) gas content, in large measure because of a general absence of adequate data on molecular gas content to apply similar tests to the galaxies in this sample. Understanding the relationship between star formation in these galaxies and their gas content, especially with regards to the global vs local stability arguments we have sketched, will require mapping of the distribution of H I and CO emission with resolution comparable to the scale of the star formation activity seen. Global arguments are inadequate for continued progress along these lines.

We wish to thank P. Hodge for suggesting this project to us in 1984, and J. C. Shields for useful discussions and a careful reading of the manuscript. We are most grateful to H. Spinrad and W. van Bruegel for the use of their interference filter set at Lick Observatory, and to the Lick Observatory TAC for generous allocations of time for this project. The research was partially supported by a grant from NASA administered by the American Astronomical Society. Observing at Lick was supported in part by the Davidson Fund at the University of California, Santa Cruz. Lick Observatory CCD instrument development was supported in part by NSF Core Block Grant No. AST-8641510. The OSU IFPS instrument project was supported by NSF Grant. Nos. AST-8822009 and AST-9112879.

REFERENCES

Aaronson, M., Huchra, J., Mould, J., Schechter, P. L., & Tully, R. B. 1982, ApJ, 258, 64
Balzano, V. 1983, ApJ, 268, 602
Benedict, G. F. 1980, AJ, 85, 513
Burstein, D., & Heiles, C. 1984, ApJS, 54, 33
Buta, R. J. 1986, ApJS, 61, 609
Caplan, J., & Deharveng, L. 1986, A&A, 155, 297
Chamaraux, P., Balkowski, C., & Fontanelli, P. 1986, A&A, 165, 15
Conti, C. 1973, ApJ, 179, 181
DaCosta, G. S. 1992, in Astronomical CCD Observing and Reduction Techniques, edited by S. B. Howell, ASP Conference Series, 23, 90
Dahari, O. A. 1985, ApJS, 57, 643
de Voucouleurs, G., de Vaucouleurs, A., Corwin, H. G., Buta, R. J., Paturel, G., & Fouqué, P. 1991, The Third Reference Catalog of Bright Galaxies (Springer, New York) (RC3)
Eder, J., Giovanelli, R., & Haynes, M. P. 1991, AJ, 102, 572
Fabbiano, G., Gioia, I. M, & Trinchieri, G. 1989, ApJ, 347, 127
Fabbiano, G., Kim, D.-W., & Trinchieri, G. 1992, ApJS, 80, 521
Feigelson, E. D., & Nelson, P. I. 1985, ApJ, 293, 192
Fisher, J. R., & Tully, R. B. 1981, ApJS, 47, 139
Fullmer, L., & Lonsdale, C. 1989, Catalogued Galaxies and Quasars Observed in the IRAS Survey, version 2 (JPL, Pasadena)
Hayes, D. S. 1970, ApJ, 159, 165
Hunter, D. 1992, private communication
Hunter, D. A., Thronson, Jr., H. A., Casey, S., & Harper, D. A. 1989, ApJ, 341, 697
Jura, M. 1986, ApJ, 306, 483
Kennicutt, R. C. 1983, ApJ, 272, 54
Kennicutt, R. C. 1989, ApJ, 344, 685
Kennicutt, R. C., Edgar, B. K., & Hodge, P. W. 1989, ApJ, 337, 761
Kennicutt, R. C., & Hodge, P. W. 1980, ApJ, 241, 573
Kennicutt, R. C., & Kent, S. M. 1983, AJ, 88, 1094
Knapp, G. R., Guhathakurta, P., Kim, D.-W., & Jura, M. 1989, ApJS, 70, 329
Koski, A. T. 1978, ApJ, 223, 56
Krann-Korteweg, R. C., & Tammann, G. A. 1979, ANac, 300, 181
Larson, R. B. 1988, in Galactic and Extragalactic Star Formation, edited by R. E. Pudritz and M. Fich, NATO ASI Series, 232 (Kluwer, Dordrecht)
Markarian, B. E., & Lipovetsky, V. A. 1971, Afz, 7, 511
Markarian, B. E., & Lipovetsky, V. A. 1973, Afz, 9, 487
Markarian, B. E., & Lipovetsky, V. A., & Stepanian, J. A. 1977, Afz, 13, 397
Markarian, B. E., & Lipovetsky, V. A., & Stepanian, J. A. 1979, Afz, 15, 201
Miller, J. S., & Mathews, W. G. 1972, ApJ, 172, 593
Oke, J. B. 1971, ApJS, 27, 21
Osterbrock, D. E. 1989, Astrophysics of Gaseous Nebulae and Active Galactic Nuclei (University Science Books, Mill Valley)
Panagia, N. 1973, AJ, 78, 929
Pogge, R. W. 1989, ApJS, 71, 433
Pogge, R. W. 1992, in Astronomical CCD Observing and Reduction Techniques, edited by S. B. Howell, ASP Conference Series, 23, p. 195
Pogge, R. W., & Eskridge, P. B. 1987, AJ, 93, 291 (PE87)
Pogge, R. W., Owen, R. M., & Atwood, B. 1992, ApJ, 399, 147
Quirk, W. J. 1972, ApJ, 176, L9
Rice, W., *et al.* 1988, ApJS, 68, 91
Sage, L. J., & Wrobel, J. M. 1989, ApJ, 344, 204
Sakka, K., Oka, S., & Wakamatsu, K. 1973, PASJ, 25, 317
Sandage, A., & Tammann, G. A. 1987, A Revised Shapley–Ames Catalog of Bright Galaxies (Carnegie Institution, Washington)
Schmidt, M. 1959, ApJ, 129, 243
Shields, J. C. 1991, AJ, 102, 1314
Siegel, S. 1956, Nonparametric Statistics for the Behavioral Sciences (McGraw Hill, New York)
Simkin, S. M., van Gorkom, J., Hibbard, J., & Su, H.-J. 1987, Science, 235, 1367
Skillman, E. D., Bothum, G. D., Murray, M. A., & Warmels, R. H. 1987, A&A, 185, 61
Smith, B. J. 1988, Ph.D. thesis, University of Massachusetts
Stetson, P. B. 1979, AJ, 84, 1056
Stover, R. J. 1986, Proceedings SPIE, 627, 195
Stover, R. J. 1988, in Instrumentation for Ground-based Optical Astronomy: Present and Future, edited by L. B. Robinson (Springer, New York), p. 443
Tacconi, L. J., Tacconi-Garman, L. E., Thornley, M., & van Woerden, H. 1992, A&A, 252, 541
Thronson, H. A., Tacconi, L., Kenny, J., Greenhouse, M. A., Margulis, M., Tacconi-Garman, L., & Young, J. S. 1989, ApJ, 344, 747
Toomre, A. 1964, ApJ, 139, 1217
Trinchieri, G., & diSerego Alighieri, S. 1991, AJ, 101, 1647
van Driel, W. 1987, Ph.D. thesis, University of Groningen
van Driel, W., & van Woerden, H. 1991, A&A, 243, 71
Wardle, M., & Knapp, G. R. 1986, AJ, 91, 23
Whitford, A. E. 1958, AJ, 63, 210
Whitmore, B. C., Lucas, R. A., McElroy, D. B., Steiman-Cameron, T. Y., Sackett, P. D., & Olling, R. P. 1990, AJ, 100, 1489
Wiklind, T., & Henkel, C. 1989, A&A, 225, 1